Electronic Supplementary Information

Engineering Framework Ti and Sn Dual Sites in Beta Zeolite via Interzeolite Transformation for Efficient Tandem Catalysis

Aohua Xiang,[a] Ziqi Zhang,[a] Yan Zhang,[a] Shufang Lv,[a] Lili Cao,[a] Sixian Shi,[a] Yan Li,[ab]* Tianjun Zhang[ab]*

[a] State Key Laboratory of New Pharmaceutical Preparations and Excipients, Key Laboratory of Medicinal Chemistry and Molecular Diagnosis of the Ministry of Education, College of Chemistry and Materials Science, Hebei University, Baoding 071002, China,

[b] State Key Laboratory of Inorganic Synthesis and Preparative Chemistry, College of Chemistry, Jilin University, Changchun 130012, China.

*Corresponding Author: Tianjun Zhang (tjzhang@hbu.edu.cn); Yan Li (liyan95@hbu.edu.cn)

Table of Contents

Experimental section

Chemical reagents

All chemicals and materials were obtained from commercial sources and used without further purification unless otherwise specified. Piperidine (PI, 99.0 wt%, Damao), fumed silica (SiO_2, 99.8 wt%, Aladdin), boric acid (H_3BO_3, 99.8 wt%, Sinopharm), tetrabutyl titanate (TBOT, 98 wt%, Sinopharm), nitric acid (HNO_3, 65.0 wt%, Damao), Tetraethylammonium hydroxide (TEAOH, 25 wt%, InnoChem), H-Beta zeolite (Si/Al=13, Nankai University Catalyst), bis(cyclopentadienyl) titanium dichloride (97 wt%, InnoChem), tin(IV) chloride pentahydrate ($SnCl_4{\cdot}5H_2O$, 99.995 wt%, Macklin), tin(II) acetate (95.0 wt%, Aladdin), ammonium fluoride (NH_4F, 99.99 wt%, InnoChem), acetonitrile (CH_3CN, 98 wt%, Macklin), ethanol (C_2H_6O, 99.7%, Sinopharm), cyclohexene (C_6H_{10}, 99.0 wt%, InnoChem), cyclopentene (C_5H_8, 98.0 wt%, InnoChem), cyclooctene (C_8H_{14}, 95.0 wt%, Aladdin), 1-methylcyclohexene (97.0 wt%, Aladdin), 1-hexene (99.0 wt%, Aladdin), 1-heptene (98.0 wt%, InnoChem), chlorobenzene (C_6H_5Cl, 99.0%, InnoChem), hydrogen peroxide solution (H_2O_2, 30%, Damao), deionized (DI) water from Clever-S30 UV water purification system (18.25 $M\Omega{\cdot}cm^{-1}$).

Materials preparation

Preparation of dealuminated Beta. Commercial H-Beta (Si/Al=13) was purchased from Nankai University Catalyst Co., Ltd. First, the parent H-Beta was calcined in air at 823 K for 6 hours, followed by refluxing in HNO_3 solution (65 wt%) at a solid-to-liquid ratio of 1 g : 20 mL for 12 hours. The acid-treated product was washed repeatedly with deionized water until pH≈7. Finally, the dried product was used as Beta seeds or used as silica source for the synthesis of TiSn-Beta-SSIE.

Preparation of Ti-MWW precursor (Ti-MWW-P) and Ti-MWW. The MWW titanosilicate was synthesized using fumed silica (SiO_2), tetrabutyl titanate (TBOT), boric acid (H_3BO_3), deionized water and piperidine (PI) as the structure-directing agent according to the literature with our slight modification.[1] Typically, PI was dissolved in deionized water at room

temperature and stirred for 30 minutes. Then, H_3BO_3 was added under stirring for 1 hour. After that, TBOT was added dropwise the solution, and the stirring was continued for 2 hours. Next, SiO_2 was added into the solution, and vigorous stirring was maintained for another 2 hours to form a homogeneous gel, with a molar composition of 1.0 SiO_2 : 0.0167 TiO_2 : 0.67 B_2O_3 : 1.4 PI : 25.0 H_2O (Si/Ti=60). The gel was transferred into a Teflon-lined autoclave and crystallized under rotation (40 rpm) at 403 K for 1 day and 443 K for 6 days. After the crystallization, the solid product was recovered by filtration and washed with deionized water until pH≈7, followed by drying at 353 K overnight, denoted as Ti-MWW precursor (Ti-MWW-P). The obtained Ti-MWW-P was refluxed with 2M HNO_3 aqueous solution for 20 hours and further calcined at 823 K for 6 hours. The Ti-MWW-P with Si/Ti=40, 80 and the B-MWW-P without Ti were also synthesized via similar procedure.

Preparation of TiSn-Beta-IT. TiSn-Beta-IT zeolite was hydrothermally synthesized via interzeolite transformation (IT) method by employing Ti-MWW-P as silica source and titanium source. In a typical synthesis, Ti-MWW-P (Si/Ti=60) powder and deionized water were added into tetraethylammonium hydroxide (TEAOH, 25 wt%) aqueous solution under stirring at room temperature for 15 minutes, resulting in a gel composition of 1.0 SiO_2: 0.0167 TiO_2: 0.5 TEAOH: 15 H_2O. Subsequently, the gel was transferred into a Teflon-lined autoclave and hydrothermally treated at 413 K for 3 hours under static condition. After quenching down to room temperature, the $SnCl_4 \cdot 5H_2O$ was added to the mixture and stirred for 10 min. Then, Beta seeds of 10 wt% with respect to silica source and the ammonium fluoride (NH_4F) were added. After that, a certain amount of water was removed at 353 K, resulting in a final molar composition of 1.0 SiO_2: 0.0152 TiO_2: 0.01 SnO_2: 0.5 TEAOH: 0.5 NH_4F: 7.5 H_2O. The mixture was further hydrothermally crystallized at 413 K for a certain time under static conditions. If not specified, the crystallization time was 2 days. The as-made product was then recovered by filtration, dried at 353 K overnight, and calcined at 873 K for 6 hours. Finally, the calcined product was denoted as TiSn-Beta-IT. For comparison, Ti-Beta-IT was synthesized via a similar route except without the addition of $SnCl_4 \cdot 5H_2O$. Sn-Beta-IT was synthesized via a similar route, using B-MWW-P instead of Ti-MWW-P. The sample designated as TiSn-Beta-IT$_{(60, 100)}$

represents the standard TiSn-Beta-IT, where 60 was the Si/Ti ratio in Ti-MWW-P and 100 was the Si/Sn ratio in final synthesis gel of TiSn-Beta-IT. The comparison samples, TiSn-Beta-IT$_{(40, 100)}$ and TiSn-Beta-IT$_{(80, 100)}$, were synthesized via the identical method but with Ti-MWW-P having Si/Ti ratios of 40 and 80, respectively.

Preparation of TiSn-Beta-SSIE. TiSn-Beta-SSIE was synthesized via a solid-state ion-exchange (SSIE) method.[2, 3] The dealuminated Beta, bis(cyclopentadienyl) titanium dichloride and tin(II) acetate were finely mixed and ground in a mortar for 30 minutes. The molar ratios of Si/Ti=60 and Si/Sn=100. Subsequently, the mixture was calcined at 823 K for 6 hours to obtain TiSn-Beta-SSIE.

Characterization methods

Powder X-ray diffraction (XRD) was performed on a Bruker D8 ADVANCE instrument with the X-ray source of Cu Kα radiation (λ = 1.5418 Å). Scanning electron microscopy (SEM) images were recorded on Thermo Scientific Apreo 2S electron microscope. Transmission electron microscopy (TEM) images were recorded on JEOL JEM-F200 electron microscope. Chemical compositions were determined with Inductively Coupled Plasma-Optical Emission Spectrometry (ICP-OES) analysis performed on Thermo Scientific iCAP PRO. Nitrogen adsorption-desorption measurements were carried out on an Autosorb-iQ-MP 3000 analyzer at 77 K. Before starting the N_2 adsorption measurements, all the samples were activated by degassing in-situ at about 473 K for 10 h. The UV-vis diffuse reflectance spectroscopy (UV-Vis DRS) over a range of 200 to 500 nm using a SHIMADZU UV-3600. X-ray photoelectron spectroscopy (XPS) was performed with an ESCALAB Xi^+ using Al as the exciting source. Raman spectra were obtained using a HORIBA LabRAM HR Evolution spectrometer with a 325 nm laser as the excitation source. Vacuum infrared (va-IR) and pyridine infrared (py-IR) spectra were recorded by Thermo Scientific Nicolet iS10 spectrometer. Prior to collecting the va-IR spectra, the zeolite self-supported wafer was outgassed in a sample cell under vacuum environment using turbo molecular pump (Pressure: 10^{-7} mbar) at 600 °C for 1 h. Then, the spectra in the hydroxyl stretching region were collected at 298 K. After the collection of va-IR spectral data, pyridine vapor was introduced into the sample cell and the outgassed wafers were placed in pyridine vapor at room temperature for 30 min. Then the py-IR spectra were collected at 323 K, 423 K, 523 K, 623 K. The data of X-ray absorption near-edge structure (XANES) and extended X-ray absorption fine structure (EXAFS) were collected at room temperature in the fluorescent mode with a Lytle detector at beamline BL14W1 and BL15U1 of the Shanghai Synchrotron Radiation Facility (SSRF, China). Data processing and EXAFS fitting were performed using the Athena, Artemis, and Igor software.

Catalytic tests

Catalytic performance was carried out in batch reactors. The catalyst was activated under vacuum at 473 K for 2 hours before used. In a typical run, 5 mmol alkene, 5 mmol H_2O_2, 5 mL acetonitrile and 100 mg catalyst were added into the batch reactor and pressurized the reactor to 3 bars of nitrogen. The reaction was carried out at 433 K for 2 hours. Sample analyses were performed on a gas chromatography with FID detector (GC, Fuli F80, HP-5 column), using chlorobenzene as an internal standard. All products were confirmed by gas chromatography-mass spectrometry (GC-MS, Agilent 8860-5977B, HP-5MS column).

The stability test of TiSn-Beta-IT was performed under the same reaction conditions as described above, except that the recycled catalyst was used. After each reaction cycle, the catalyst powder was washed several times with ethanol, then dried at 353 K overnight and calcined in air at 823 K for 6 hours for the next use.

Supplementary figures and tables

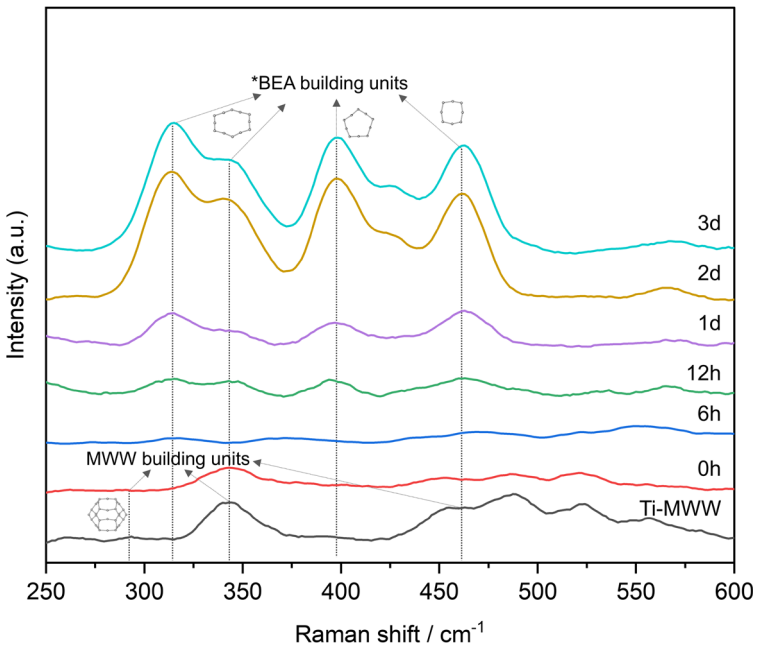

Figure S1 UV-Raman spectra of Ti-MWW and TiSn-Beta solid products obtained from 0 h to 3 d.

Note: The structural reconstruction was corroborated by Raman spectroscopy. The Ti-MWW zeolite exhibits characteristic bands around 290, 340, and 460 cm^{-1}, which are associated with double six-membered ring (D6R), six-membered rings (6MR), and four-membered rings (4MR), respectively.[4] After hydrothermal treatment in TEAOH, these features are markedly attenuated, consistent with substantial degradation of the Ti-MWW framework in XRD. Upon 6 h of crystallization, new weak bands assignable to 4MR (464 cm^{-1}), 5MR (398 cm^{-1}), and 6MR (315 and 345 cm^{-1}) appear, which are widely regarded as primary structural motifs for the *BEA topology.[5, 6] As crystallization proceeds, these Raman bands progressively sharpen and intensify, and their intensities become essentially invariant after 2 days, in good agreement with the XRD-derived crystallinity plateau, indicating the complete construction of the *BEA framework.

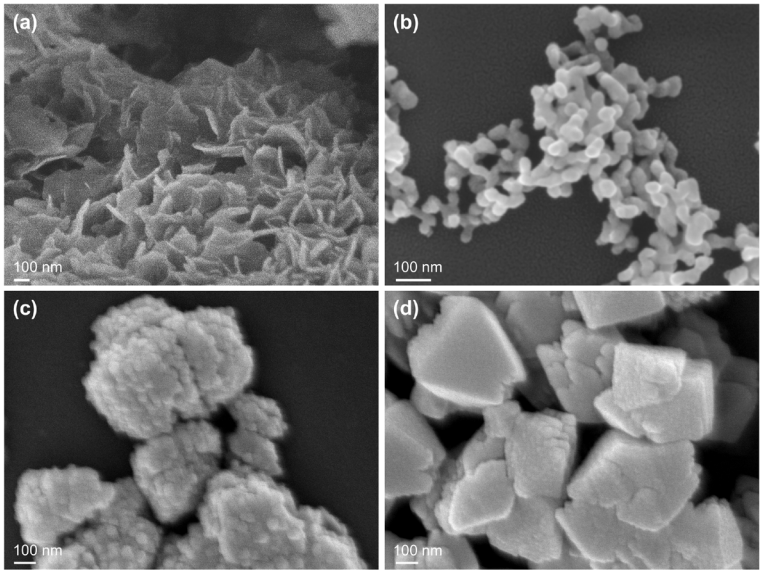

Figure S2 SEM images of (a) Ti-MWW-P and (b-d) the corresponding TiSn-Beta solid products obtained from 0 h, 12 h, 2 d.

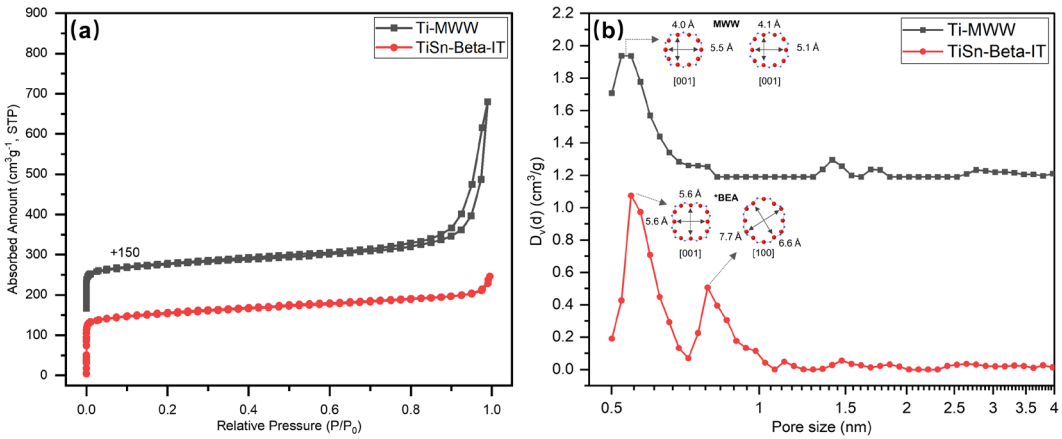

Figure S3 (a) N_2 adsorption and desorption isotherms and (b) pore size distributions of Ti-MWW and TiSn-Beta-IT.

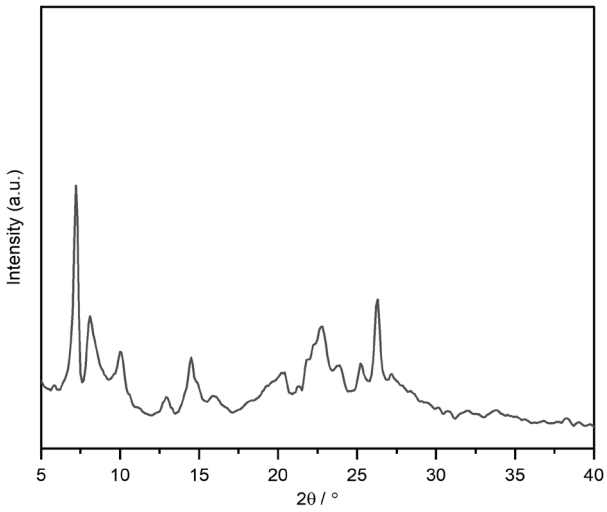

Figure S4 XRD pattern of Ti-MWW zeolite.

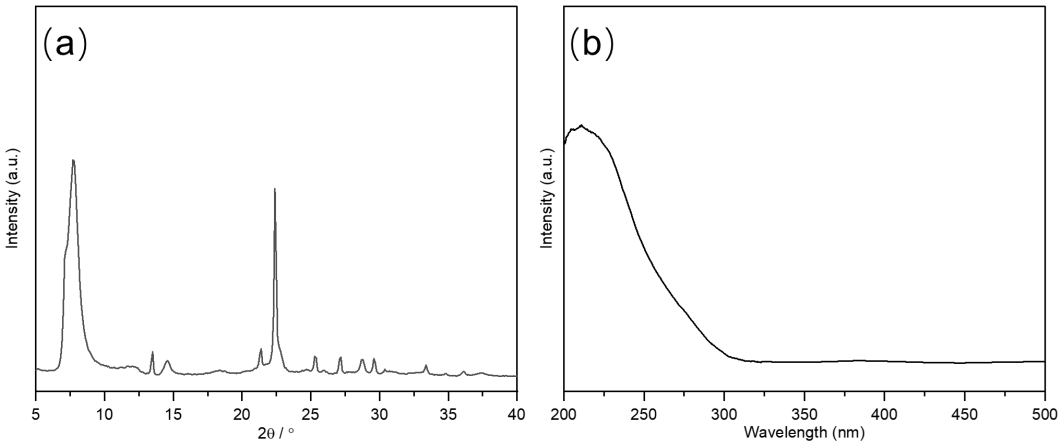

Figure S5 (a) XRD pattern and (b) UV-vis spectra of Ti-Beta-IT.

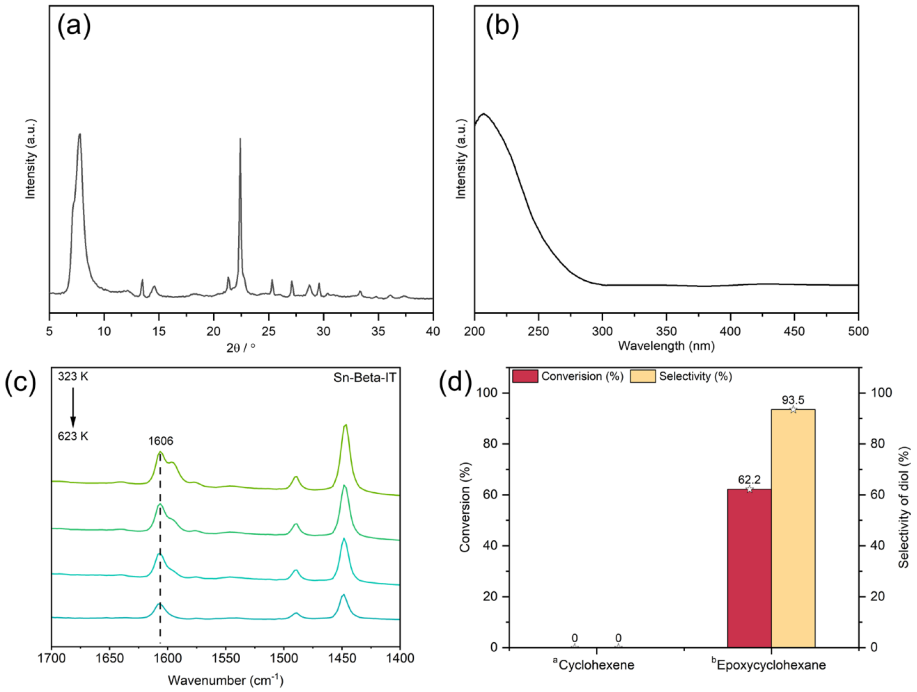

Figure S6 (a) XRD pattern, (b) UV-vis spectra, (c) py-IR spectra at 323 K, 423 K, 523 K, 623 K of Sn-Beta-IT; (d) Cyclohexene and epoxycyclohexane conversion over Sn-Beta-IT.

[a] Reaction conditions: cat., 100 mg; cyclohexene, 5 mmol; H_2O_2 (30 wt %), 5 mmol; CH_3CN, 5 mL; temp., 333 K; time, 2 h; 3 bar of N_2.

[b] Reaction conditions: cat., 100 mg; epoxycyclohexane, 5 mmol; H_2O 1 mL; temp., 333 K; time, 2 h; 3 bar of N_2.

Note: As shown in Figure S6 a and S6 b, Sn-Beta with fully incorporated framework Sn species was successfully synthesized via the interzeolite transformation method. In addition, the py-IR spectrum of Sn-Beta-IT (Figure S6 c) exhibits a distinct absorption band at 1606 cm^{-1}, which is characteristic of pyridine coordinated to Lewis acid sites. Moreover, this band is well-preserved even after desorption at elevated temperatures (indicating the high thermal stability of the adsorbed pyridine), which confirms the presence of strong Lewis acid sites in Sn-Beta-IT. As shown in the Figure S6d, Sn-Beta-IT exhibits negligible activity in the one-pot tandem conversion of cyclohexene, with no products detected. This confirms that Sn sites alone cannot activate H_2O_2 to initiate the epoxidation of cyclohexene (the first step). Notably, Sn-Beta-IT achieves a high epoxycyclohexane conversion of 62.2 % with a 1,2-cyclohexanediol selectivity of 93.5% within 2 h. This result supports the mechanism that framework Sn species serve as the key Lewis acid centers for the second epoxide hydration step.

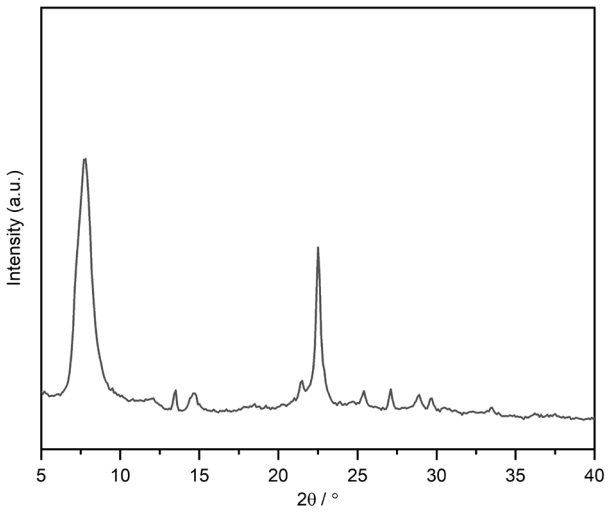

Figure S7 XRD pattern of TiSn-Beta-SSIE

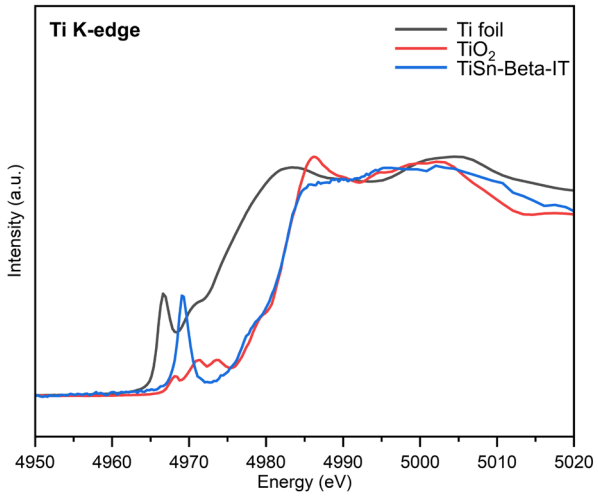

Figure S8 Ti K-edge XANES spectra of TiSn-Beta-IT and corresponding standards.

Note: The Ti K-edge X-ray absorption near-edge structure (XANES) was employed to qualitatively probe the local coordination symmetry of Ti species by comparing the pre-edge peaks (approx. 4960–4980 eV) with those of Ti foil and TiO_2 (anatase). In general, the intensity of the pre-edge peak is highly sensitive to the coordination geometry; specifically, tetrahedral Ti species typically exhibit a sharp and intense pre-edge feature due to p-d orbital mixing.[7] As shown in Figure S8, TiSn-Beta-IT displays a distinct, intense single peak, confirming the dominance of TiO_4. Furthermore, the absence of distinct scattering features in the post-edge region suggests a lack of long- or medium-range ordered Ti-O-Ti structures, indicating that Ti species are highly dispersed in TiSn-Beta-IT.

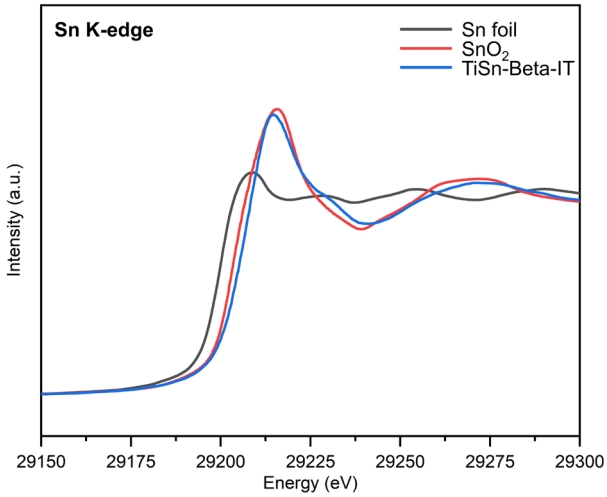

Figure S9 Sn K-edge XANES spectra of TiSn-Beta-IT and corresponding standards.

Note: In Figure S9, the XANES edge position and white line height of TiSn-Beta-IT closely resemble those of SnO_2, indicating that Sn is present as Sn(IV) with four oxygen nearest neighbors.[8]

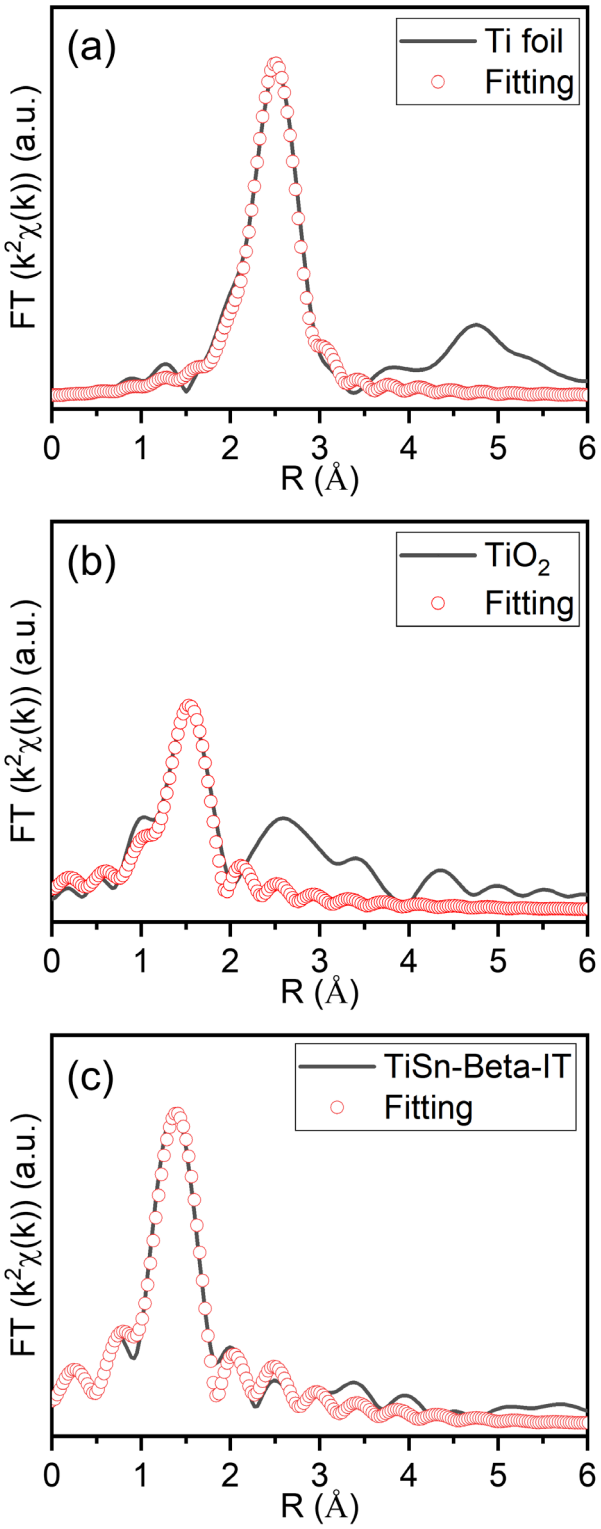

Figure S10 Ti K-edge FT-EXAFS and fitting curves of (a) Ti foil, (b) anatase TiO_2, (c) TiSn-Beta-IT.

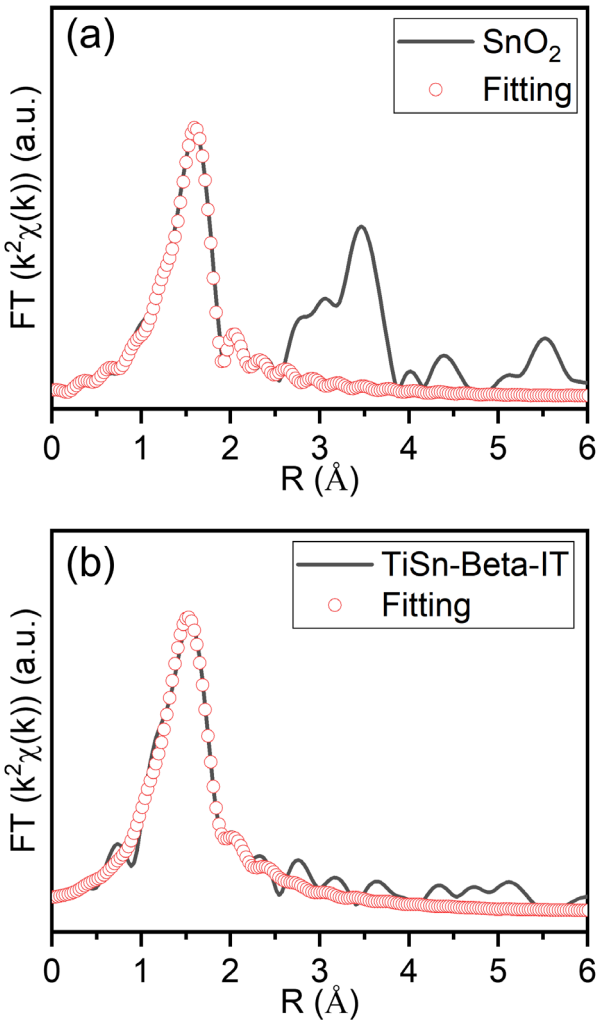

Figure S11 Sn K-edge FT-EXAFS and fitting curves of (a) SnO_2, (b) TiSn-Beta-IT.

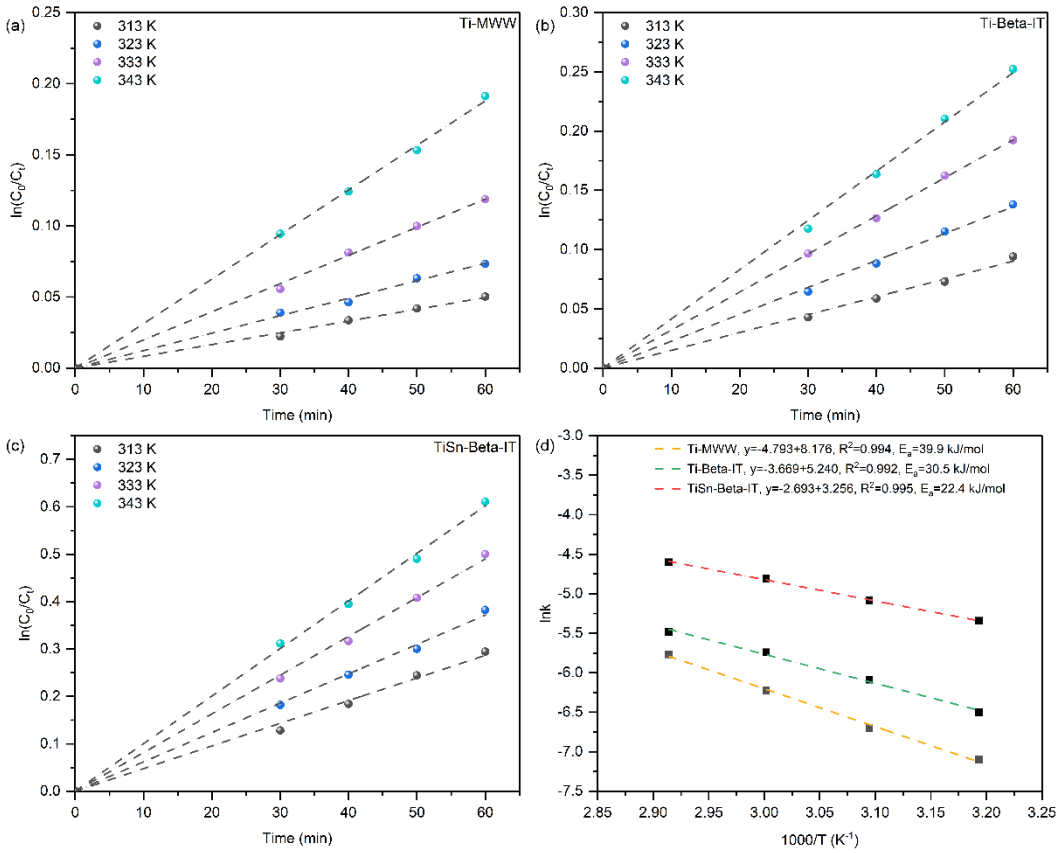

Figure S12 Kinetic analysis of cyclohexene conversion of (a) Ti-MWW, (b) Ti-Beta-IT and (c) TiSn-Beta-IT; (d) plots of apparent activation energy of different catalysts.

Note: As shown in Fig. S12 a-c, a linear relationship between the natural logarithm of cyclohexene concentration (ln C) and the reaction time (t) is observed at various temperatures (313-343 K), indicating that the reaction follows pseudo-first-order kinetics.

The apparent activation energy (*Ea*) is then calculated using the Arrhenius equation. As shown in Fig. S12 d, compared to Ti-MWW (*Ea* = 39.9 kJ/mol), Ti-Beta-IT exhibits a lower *Ea* (30.5 kJ/mol), demonstrating the enhanced catalytic activity of Ti species within the *BEA framework compared to those in the MWW framework. Furthermore, with the simultaneous incorporation of Ti and Sn active sites via interzeolite transformation, the *Ea* further decreases to 22.4 kJ/mol for TiSn-Beta-IT. This result indicates a synergistic effect between the Ti and Sn sites in TiSn-Beta-IT, which effectively lowers the energy barrier and promotes the conversion of cyclohexene.

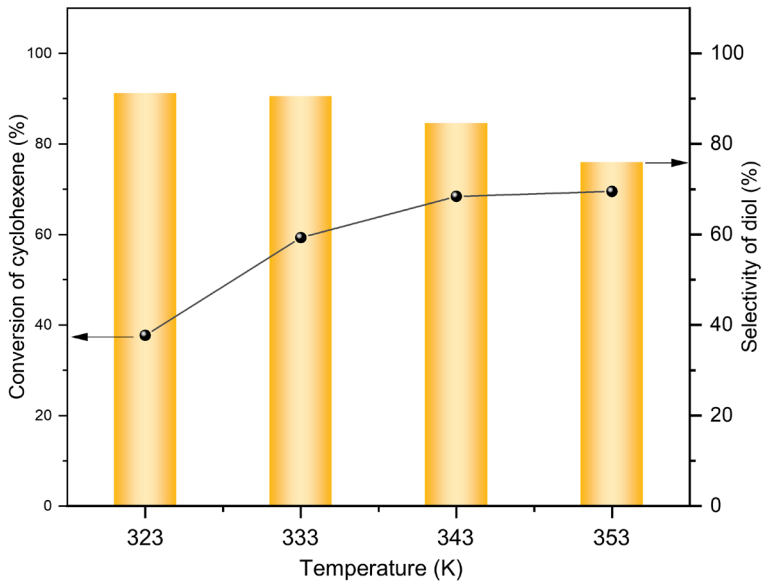

Figure S13 Effect of temperature on the conversion of cyclohexene to 1, 2-cyclohexanediol over TiSn-Beta-IT.

Note: The effect of reaction temperature on the catalytic activity of TiSn-Beta-IT was studied. Increasing the temperature improved cyclohexene conversion but compromised the selectivity for 1,2-diol. This is likely due to the promotion of side reactions, yielding byproducts such as cyclohex-2-en-1-ol and cyclohex-2-en-1-one.

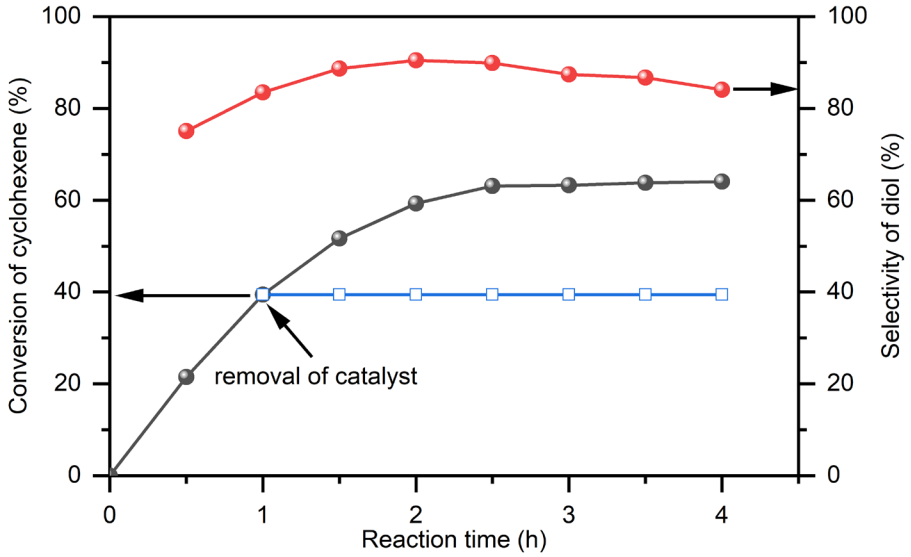

Figure S14 Effect of reaction time on the conversion of cyclohexene to 1, 2-cyclohexanediol over TiSn-Beta-IT.

Note: The conversion of cyclohexene over TiSn-Beta-IT increased within the first 2.5 h and then plateaued (remained essentially unchanged), whereas the selectivity for 1,2-diol decreased slightly after 2 h. Furthermore, we remove the catalyst from the reaction mixture by centrifugation after 1 h, and the reaction is monitored for another 3 h. The removal of the catalyst lead to the complete termination of the reaction, confirming that no active Ti and Sn sites leach into the reaction solution. Furthermore, neither Ti nor Sn is detected in the reaction solution by ICP, so the possibility of leaching can be excluded.

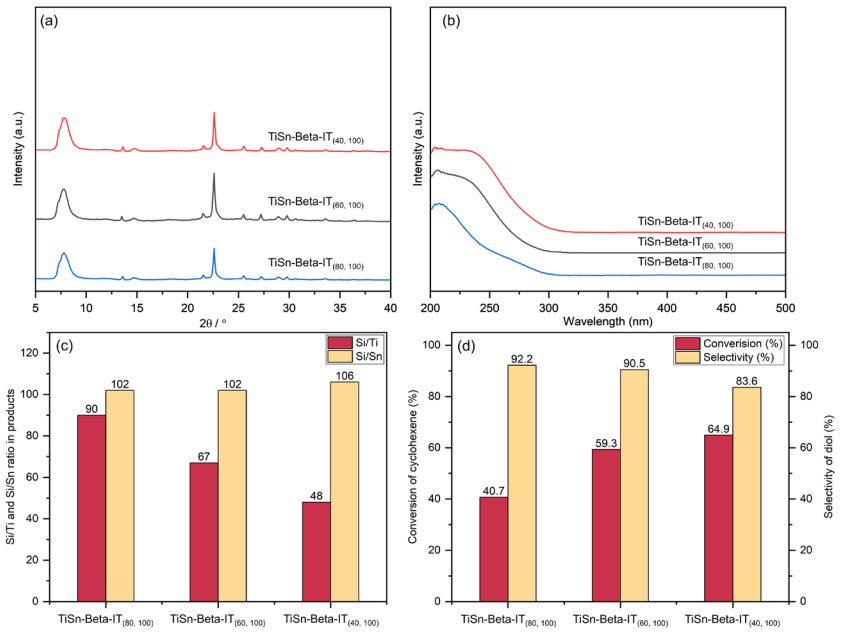

Figure S15 (a) XRD patterns, (b) UV-vis spectra, (c) Si/Ti and Si/Sn ratio in solid products determined by ICP-OES of different TiSn-Beta-IT$_{(x, y)}$ zeolites, (d) catalytic performance on the conversion of cyclohexene to 1, 2-cyclohexanediol over different TiSn-Beta-IT$_{(x, y)}$ zeolites. x represents the Si/Ti ratio in Ti-MWW-P (varied among 80, 60, 40), y represents the Si/Sn ratio in synthesis gel (fixed as 100).

Note: A series of TiSn-Beta-IT zeolites was successfully synthesized by varying the Si/Ti ratio (80, 60, and 40) while maintaining a fixed Si/Sn ratio of 100. XRD patterns indicate that all samples are well-crystallized. The successful framework incorporation of Ti and Sn was confirmed by UV-vis spectroscopy and ICP analysis. Notably, increasing the Ti content gradually enhanced cyclohexene conversion; however, higher Ti loading (Si/Ti = 40) resulted in the generation of excessive byproducts.

More specifically, As shown in Fig. S15c and d, the effect of Ti content on the catalytic performance is investigated systematically. Comparing TiSn-Beta-IT$_{(60, 100)}$ with TiSn-Beta-IT$_{(80, 100)}$, the Ti content (detected by ICP) is increased by 34.3%, resulting in a 45.7% increase in the conversion of cyclohexene. This sharp rise is attributed to the formation of abundant Ti-Sn synergistic active sites.

In contrast, a further increase in Ti content yields diminishing returns. When the Ti loading (detected by ICP) is further increased by 39.6% (comparing TiSn-Beta-IT$_{(40, 100)}$ with TiSn-Beta-IT$_{(60, 100)}$), the conversion only increases by 9.4%. Since the Sn content is fixed (Si/Sn=100), the number of potential Ti-Sn synergistic active sites is limited. Once the Sn sites are saturated with proximal Ti, excess Ti species likely exist as isolated sites rather than synergistic active sites, resulting in only a marginal improvement in activity. This confirms that the Ti-Sn synergy is the primary driver for the high catalytic performance.

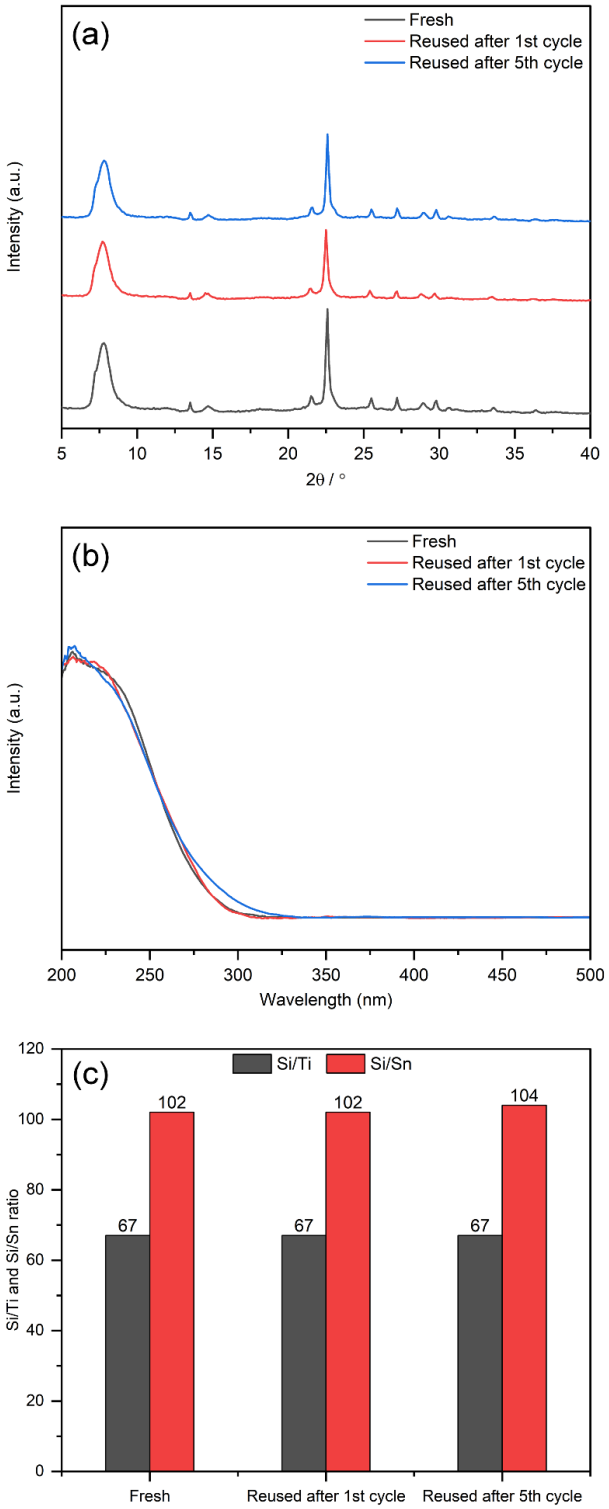

Figure S16 (a) XRD patterns, (b) UV-vis spectra and (c) ICP-OES results for fresh and reused TiSn-Beta-IT catalysts.

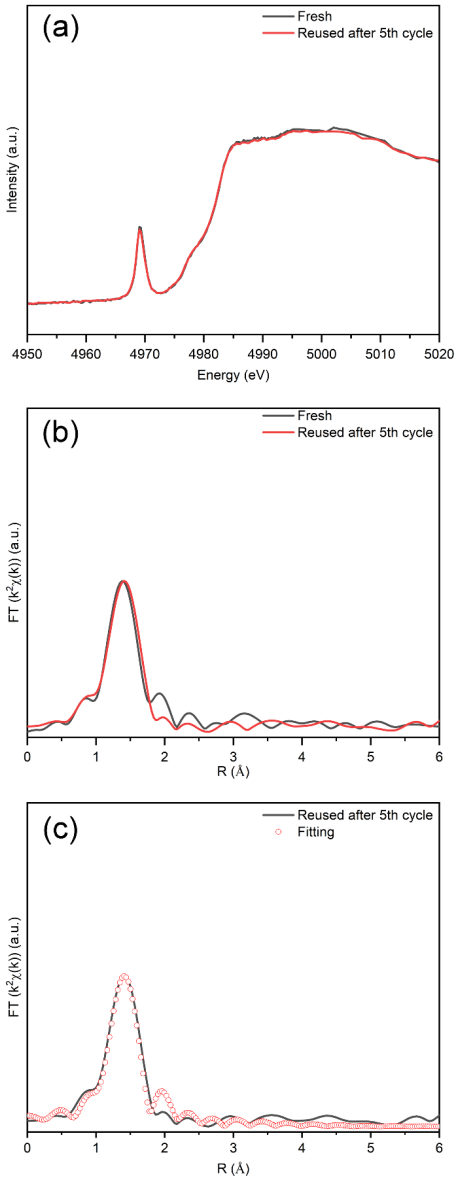

Figure S17 (a) XANES spectra, (b) FT-EXAFS spectra of fresh and reused TiSn-Beta-IT catalyst; (c) FT-EXAFS fitting curve of reused TiSn-Beta-IT catalysts.

Note: As shown in revised Fig. S17, the XANES spectrum of the reused sample (after 5 cycles) is overlapped well with that of the fresh TiSn-Beta-IT, indicating that the local symmetry and oxidation state of the Ti species remained unchanged. Moreover, the FT-EXAFS results show that the Ti-O bond length is consistent before and after the reaction. The EXAFS fitting results (Table S6) further confirm that the coordination number of the Ti-O bond in the reused sample (4.0) is similar to that of the fresh TiSn-Beta-IT (4.1). These results firmly demonstrate that the coordination environment of the framework Ti species was well-preserved, confirming the high stability of the framework Ti active sites during the reuse process.

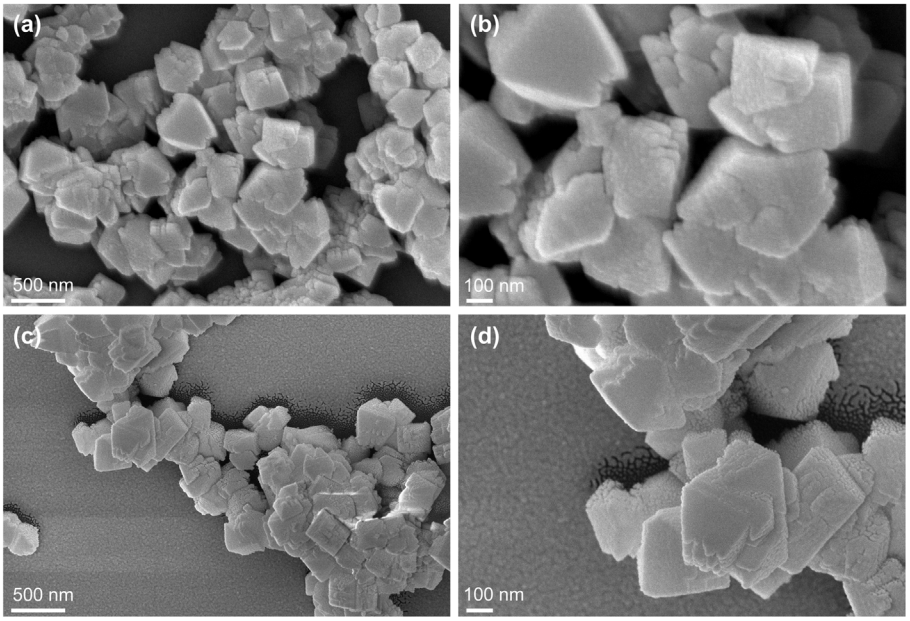

Figure S18 SEM images of TiSn-Beta-IT (a, b) fresh and (c, d) after 5 cycles.

Table S1 Textural properties of different zeolites

Samples	S_{BET} (m^2/g)[a]	S_{micro} (m^2/g)[b]	S_{ext} (m^2/g)[b]	V_{micro} (cm^3/g)[b]	V_{total} (cm^3/g)[c]	V_{meso} (cm^3/g)[d]
Ti-MWW	468	340	128	0.14	0.82	0.68
TiSn-Beta-IT	584	455	129	0.18	0.38	0.20

[a] S_{BET} (total surface area) calculated using the BET method; [b] S_{micro} (micropore area), S_{ext} (external surface area) and V_{micro} (micropore volume) calculated using the t-plot method. [c] Total pore volume at $P/P_0 = 0.995$. [d] $V_{meso} = V_{total} - V_{micro}$.

Table S2 Quantify of Ti and Sn species in TiSn-Beta-IT and TiSn-Beta-SSIE via XPS fitting.

	Ti 2p		Sn 3d	
	FW TiO_4 (%)	EFW TiO_2 (%)	FW SnO_4 (%)	EFW SnO_2 (%)
TiSn-Beta-IT	100	-	100	-
TiSn-Beta-SSIE	43	57	38	62

FW: framework; EFW: Extra-framework.

Table S3 Fitting parameters of EXAFS spectra at Ti K-edge and Sn K-edge for TiSn-Beta-IT and corresponding standards.

Sample	Shell	C.N.	R (Å)	σ^2 (Å)	E_0 (eV)	R-factor (%)
Ti foil	Ti-Ti	12.0	2.89±0.01	0.007±0.001	4.6±0.8	1.4
TiO_2	Ti-O	6.0	1.94±0.02	0.002±0.003	2.2±3.9	2.2
TiSn-beta-IT	Ti-O	4.1±0.8	1.82±0.02	0.002±0.001	8.4±2.4	1.7
TiSn-beta-IT	Sn-O	4.3±0.3	2.00±0.01	0.007±0.001	4.5±0.8	0.6
SnO_2	Sn-O	6.0	2.05±0.01	0.003±0.001	6.5±0.8	0.8

C.N., coordination number; R, the distance between absorber and backscatter atoms. σ^2 is Debye-Waller factor (a measure of thermal and static disorder in absorber-scatterer distances); ΔE_0 is an edge-energy shift (the difference between the zero-kinetic energy value of the sample and that of the theoretical model).

Table S4 Si/Ti and Si/Sn ratio of different zeolite.

Sample	Si/Ti		Si/Sn	
	Gel	Product[a]	Gel	Product[a]
Ti-MWW-P	60	61	-	-
Ti-MWW	60[b]	68	-	-
TiSn-Beta-IT	60[b]	67	100	102
TiSn-Beta-SSIE	60	64	100	101
Ti-Beta-IT	60[b]	66	-	-
Sn-Beta-IT	-	-	100	101

[a] Determined by ICP-OES.

[b] Based on the Ti-MWW-P.

Table S5 Tandem catalytic activity of TiSn-Beta-IT in the transformation of various olefins into the corresponding 1,2-diols.

Substrates	Conv. (%)	Select. (%)
Cyclopentene	67.1	81.4
Cyclohexene	59.3	90.5
Cyclooctene	41.5	96.3
1-Methylcyclohexene	47.6	79.2
1-Hexene	61.2	75.8
1-Heptene	65.4	73.5

Reaction conditions: cat, 100 mg; alkenes, 5 mmol; H_2O_2 (30 wt %), 5 mmol; CH_3CN, 5 mL; temp., 333 K; time, 2 h; 3 bar of N_2.

Table S6 Fitting parameters of EXAFS spectra at Ti K-edge for fresh and reused TiSn-Beta-IT

Sample	Shell	C.N.	R (Å)	σ^2 (Å)	E_0 (eV)	R-factor (%)
Fresh TiSn-Beta-IT	Ti-O	4.1±0.8	1.82±0.02	0.002±0.001	8.4±2.4	1.7
Reused TiSn-Beta-IT	Ti-O	4.0±0.8	1.82±0.02	0.002±0.002	6.2±2.0	1.8

C.N., coordination number; R, the distance between absorber and backscatter atoms. σ^2 is Debye-Waller factor (a measure of thermal and static disorder in absorber-scatterer distances); ΔE_0 is an edge-energy shift (the difference between the zero-kinetic energy value of the sample and that of the theoretical model).

References

1. P. Wu, T. Tatsumi, T. Komatsu and T. Yashima, *J. Phys. Chem. B*, 2001, **105**, 2897-2905.
2. Z. Yang, Q. Yu, Y. Guo, X. Wu, H. Wang, J. Han, Q. Ge and X. Zhu, *Microporous Mesoporous Mater.*, 2022, **330**, 111625.
3. A. Al-Nayili, K. Yakabi and C. Hammond, *J. Mater. Chem. A*, 2016, **4**, 1373-1382.
4. Z. Zhu, H. Xu, B. Wang, J. Yin, J. Jiang, H. Lü and P. Wu, *Chem. Commun.*, 2019, **55**, 14279-14282.
5. H. Ma, Z. Zhu, P. Tang, T. Su, P. Wu and H. Lü, *Microporous Mesoporous Mater.*, 2021, **311**, 110702.
6. W. Fu, Z. Yuan, S. Jin, W. Liu, Z. Wang, C. Wang, Y. Wang, W. Yang and M. Y. He, Chin. *J. Catal.*, 2019, **40**, 856-866.
7. N. G. Lefton and A. T. Bell, *ACS Catal.*, 2024, **14**, 3986-4000.
8. M. Signorile, L. Braglia, V. Crocellà, P. Torelli, E. Groppo, G. Ricchiardi, S. Bordiga and F. Bonino, *Angew. Chem. Int. Ed.*, 2020, **59**, 18145-18150.